Sensorless Temperature Monitoring of Lithium-ion Batteries by Integrating Physics with Machine Learning

Zheng, Yusheng; Che, Yunhong; Hu, Xiaosong; Sui, Xin; Teodorescu, Remus

Published in:
IEEE Transactions on Transportation Electrification

DOI (link to publication from Publisher):
10.1109/tte.2023.3294417

Publication date:
2024

Document Version
Accepted author manuscript, peer reviewed version

Sensorless Temperature Monitoring of Lithium-ion Batteries by Integrating Physics with Machine Learning

Yusheng Zheng, *Graduate Student Member IEEE*, Yunhong Che, *Graduate Student Member IEEE*, Xiaosong Hu, *Senior Member, IEEE*, Xin Sui, *Member, IEEE*, Remus Teodorescu, *Fellow, IEEE*

***Abstract*—The large-scale application of lithium-ion batteries in electric vehicles requires meticulous battery management to guarantee vehicular safety and performance. Temperatures play a significant role in the safety, performance, and lifetime of lithium-ion batteries. Therefore, the state of temperature (SOT) of batteries should be monitored timely by the battery management system. Due to limited onboard temperature sensors in electric vehicles, the SOT of most batteries must be estimated through other measured signals such as current and voltage. To this end, this paper develops an accurate method to estimate the surface temperature of batteries by combing the physics-based thermal model with machine learning. A lumped-mass thermal model is applied to provide prior knowledge of battery temperatures for machine learning. Temperature-related feature, such as internal resistance, is extracted in real-time and fed into the machine learning framework as supplementary inputs to enhance the accuracy of the estimation. A machine learning model, which combines a convolutional neural network with a long short-term memory neural network, is sequentially integrated with the thermal model to learn the mismatch between the model outputs and the real temperature values. The proposed method has been verified against experimental results, with accuracy improvement of 79.37% and 86.24% compared to conventional pure thermal model-based and pure data-driven approaches respectively.**

***Index Terms*—Electric mobilities, lithium-ion batteries, temperature estimation, thermal models, machine learning.**

I. Introduction

TRANSPORTATION electrification is one of the most promising ways to realize sustainable energy development. As the predominant energy storage component in electric mobilities such as electric vehicles (EVs) and electric aircraft, lithium-ion batteries (LIBs) exhibit superiority in energy and power density, cycle life, and charge/discharge efficiency compared with previous generations of batteries [1], [2]. The ever-increasing use of LIBs in transportation applications leads to higher requirements for battery safety and performance [3]. Nevertheless, owing to the highly nonlinear temperature characteristic of LIBs, it becomes difficult to manage battery safety, performance, and lifetime in EVs. Specifically, high temperatures increase the risk of safety hazards such as thermal runaways, which might cause catastrophic loss [4]. Low temperatures undermine the energy and power capability of LIBs by causing sluggish electrochemistry inside the cell [5]. Both low and high temperatures can contribute to accelerated battery degradation, with lithium plating triggered by the former factor and the growth of solid electrolyte interphase (SEI) caused by the latter [6]. In this context, it is of paramount importance to regulate the battery temperature to an optimal range through active thermal control [5], [7], during which accurate monitoring of battery temperature serves a fundamental role.

Typically, the temperature of LIBs can be measured directly by the surface-mounted temperature sensors in the EV battery pack. Nevertheless, it is impossible to install a temperature sensor at the surface of each cell to monitor its temperature since this will inevitably increase the cost and hardware complexity of the battery pack, especially when the pack consists of hundreds and even thousands of cells [8]. It has been reported that the average temperature sensors-to-cell ratio in an EV battery pack is around 1/10, which means that the temperature information of the majority of the cells cannot be obtained directly through measurements [8]. However, temperature abnormity might still occur in those cells without surface-mounted temperature sensors and such abnormity can hardly be detected by temperature sensors installed on nearby cells. Therefore, tracking the SOT of those cells by taking advantage of non-temperature signals such as current and voltage is of paramount importance to the safety and performance of the whole battery pack in EVs, which makes this work different from existing SOT estimation/prediction studies relying on a surface temperature sensor [9]–[12].

This work was partially supported by the Villum Foundation for Smart Battery project (No. 222860), and the National Natural Science Foundation of China (No. 52111530194) (*Corresponding authors: Yunhong Che, Xiaosong Hu*).

Yusheng Zheng, Yunhong Che, Xin Sui, Remus Teodorescu are with the Department of Energy, Aalborg University, Aalborg 9220, Denmark (e-mail: yzhe@energy.aau.dk; ych@energy.aau.dk; xin@energy.aau.dk; ret@energy.aau.dk)

Xiaosong Hu is with the College of Mechanical and Vehicle Engineering, Chongqing University, Chongqing 400044, China (e-mail: xiaosonghu@ieee.org).

Generally, there are three main methods to achieve sensorless SOT estimation in the existing literature, based on battery impedance [13]–[15], battery thermal models [16]–[18], and machine learning (ML) algorithms [19]–[21]. In impedance-based estimation, the relationship between battery temperature and impedance parameters (e.g., real part, imaginary part, and phase) will be calibrated offline by selecting an optimal frequency under which the impedance parameters are sensitive to battery temperature while insensitive to the state of charge (SOC) and state of health (SOH) [22], [23]. Afterward, the parameterized impedance-temperature relationship will be applied to estimate battery temperature according to the measured impedance online. As for thermal model-based estimation, various simplified thermal models can be developed to capture battery thermal dynamics such as heat generation, heat accumulation, and heat dissipation online [16]–[18]. Closed-loop observers are designed based on simplified thermal models to estimate battery temperature through voltage or impedance feedback [17], [24]. Regarding data-driven estimations, mature ML algorithms like artificial neural networks (ANNs) can be applied to recognize the underlying data pattern between measurements and battery temperatures by ignoring the complicated thermal dynamics of LIBs [19]–[21]. Nevertheless, the aforementioned three methods have limitations. For impedance-based estimations, the need for excitation equipment increases the hardware cost and complexity. Furthermore, batteries need to be at a close-to-equilibrium state for precise impedance measurement, which requires sufficient relaxation time before measurement and makes it difficult to capture battery temperature timely [17]. For thermal model-based estimation, how to strike a balance between the model accuracy, complexity, and parameterization difficulty is a key issue. Simple thermal models are lightweight but may suffer from poor accuracy [25]. Complex thermal models can achieve high accuracy, yet will increase the computational burden and parameterization difficulty [25]. For data-driven estimation, the generalization capability of the algorithm is always the biggest concern despite high accuracy. Moreover, data-driven methods are not able to achieve accurate estimation when prior knowledge of the battery temperature is lacking [10].

In recent years, physics-informed machine learning (PIML), as a way of integrating physical information and ML techniques, exhibits great potential in addressing the aforementioned problems [26]. To this end, this paper develops a sensorless surface temperature estimation method for LIBs by combining physics-based models and ML algorithms to leverage their respective strengths. In this way, both the estimation accuracy and generalization ability can be guaranteed. Specifically, a lumped-mass thermal model, with the advantages of being simple, physically identifiable, and less susceptible to overfitting, is established to capture the thermal dynamics of LIBs and provide prior knowledge of battery temperature for the ML algorithms. Temperature-related features, such as internal resistance, can be extracted timely and treated as inputs to the ML algorithm to further increase the estimation accuracy. Finally, a combined convolutional neural network (CNN)-long short-term memory (LSTM) neural network, is leveraged to learn the mismatch between the physics-based models and the real battery temperature so that the estimation errors caused by unmodeled thermal dynamics and parameterization errors can be further reduced.

The remainder of this article is organized as follows. Section II introduces the proposed methodology for sensorless temperature estimation. Section III describes the datasets used in this work. Next, the results and discussions are presented in Section IV, followed by the main conclusion in Section V.

II. Framework for Sensorless Surface Temperature Estimation

This section presents the framework for sensorless surface temperature estimation. The lumped-mass thermal model of LIBs, the online identification of the battery's internal resistance, and the CNN-LSTM will be introduced in detail. Then, the way of integrating physics with CNN-LSTM will be elucidated.

A. Lumped-mass Thermal Model

The lumped-mass thermal model is a simplified model used to capture the temperature response of the battery. This model regards the battery cell as a single particle, and the temperature gradient inside the cell is neglected so that the thermal dynamics of the cell can be represented by its bulk temperature. With this assumption, the governing equation for energy balance can be expressed as follows:

$$mC_p \frac{dT}{dt} = Q - hA\left(T - T_f\right) \tag{1}$$

where m, C_p, and A are the mass, heat capacity, and surface area of the battery cell, respectively; T is the time-varying temperature of the cell during operations (can be substituted with surface temperature T_s in this study), t is time, Q is the total heat generation rate of the cell, h is the equivalent convective heat transfer coefficient from the battery cell to the coolant, T_f is the coolant temperature. Here, the radiation heat dissipation is not considered since it is negligible compared to convective heat dissipation, owing to the low emissivity of the battery case, small geometric size, and relatively low operating temperature (−30 ℃ - 60 ℃) [25].

The heat generation inside the cell consists of ohmic heat, polarization heat, and various electrochemical reaction heat [27]. The complete heat generation equation contains numerous electrochemical parameters which are onerous to be obtained in real applications. Therefore, a simplified equation can be used to capture the internal heat generation of the cell, which is expressed as [28]:

$$Q = I\left(V_t - V_{oc}\right) + IT\frac{\partial V_{oc}}{\partial T} \tag{2}$$

where I, V_{oc}, and V_t denote the current (positive for charging and negative for discharging), open circuit voltage (OCV), and terminal voltage, respectively, $\partial V_{oc}/\partial T$ is the entropic heat coefficient corresponding to the entropy change during

electrochemical reactions. The total heat generation consists of irreversible heat and reversible heat, denoted by the first and the second terms respectively at the right-hand side of Eq. (2). Under high-rate operations, the reversible heat can be neglected due to its small contributions.

Although the lumped-mass thermal model was pointed out to have the lowest accuracy and may lead to unfavorable oversimplification of the battery thermal dynamics [25], it is simple enough with its parameters being easily identifiable and less prone to overfitting. Most importantly, despite rough accuracy, the model can capture the trend of battery temperature under various operating conditions since it is developed based on first principles. The estimated battery temperature and the calculated heat generation by the thermal model can provide some prior thermal information for the ML algorithm.

B. Online Internal Resistance Identification

For sensorless SOT estimation, only the current, voltage, and coolant temperature are measurable. Hence, it is important to extract some temperature-related features that can reflect the current battery SOT from these signals. By adding these features to the estimation loop, the estimation accuracy can be improved. According to ref. [18], the internal resistance of the battery is more sensitive to temperature change than voltage and therefore it can be used as a temperature-related feature.

Owing to the complex electrical dynamics, a battery cell cannot be regarded as pure resistance. In this regard, the internal resistance of the battery should be extracted based on an electrical model that captures the electrical behavior of the cell. The first-order equivalent circuit model (ECM), with its parameters being easily identified, can be applied in this work. This model consists of an OCV, an ohmic resistor R_0, and a resistor-capacitor (RC) pair, as illustrated in Fig. 1.

Assuming the constant value of model parameters during a sampling period, the terminal voltage of the battery V_t in first-order ECM can be expressed as [29],

$$\begin{aligned} V_t(t) &= V_{oc}(SOC) + (R_0 + R_1) I(t) \\ &+ R_0 R_1 C_1 \frac{dI(t)}{dt} - R_1 C_1 \frac{dV_t(t)}{dt} + w(t) \end{aligned} \tag{3}$$

where V_1 is the voltage across the RC pair, V_{oc} varies with battery SOC and can be obtained through experiments, the current $I(t)$ is positive for charging and negative for discharging, $w(t)$ denotes the noise in the model represented by some unmodeled battery dynamics and can be expressed as,

$$w(t) = \sum_{i=1}^{n_d} c_i(t) n(t-i) + n(t) \tag{4}$$

in which n_d is the order of the noise model, $c_i(t)$ is the coefficient, and $n(t)$ is the white noise, which represents the random error of the first-order ECM, and $n(t-1)$,…, $n(t-n_d)$ are its regressive values.

With the first-order ECM, the internal resistance of the battery can be extracted in real time through online identification. Particularly, this study adopts the method proposed by Feng et al. [29] based on the recursive extended least squares (RELS) algorithm. To realize online identification, Eq. (3) can be further expressed as a parametric model,

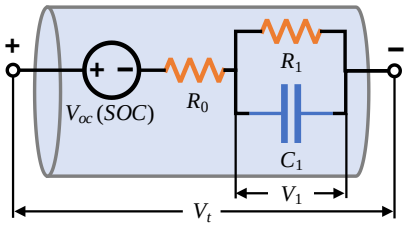

Fig. 1. Schematic of first-order ECM for LIBs.

$$y(t) = \boldsymbol{\Phi}^T(t)\boldsymbol{\theta}(t) + n(t) \tag{5}$$

where we have output $y(t)$, parameters $\boldsymbol{\theta}(t)$, and input $\boldsymbol{\Phi}(t)$ defined as follows:

$$\begin{cases} y(t) = V_t(t) - V_{oc} \\ \boldsymbol{\theta}(t) = \left[\theta_1(t), \theta_2(t), \theta_3(t), c_1(t), \cdots, c_{n_d}(t)\right]^T \\ \quad\quad = \left[(R_0 + R_1), R_0 R_1 C_1, -R_1 C_1, c_1(t), \cdots, c_{n_d}(t)\right]^T \\ \boldsymbol{\Phi}(t) = \left[I(t), \dfrac{dI(t)}{dt}, \dfrac{dV_t(t)}{dt}, n(t-1), \cdots, n(t-n_d)\right]^T \end{cases} \tag{6}$$

in which $dI(t)/dt$ and $dV_t(t)/dt$ are approximated by $\left[I(t) - I(t-\Delta t)\right]/\Delta t$ and $\left[V_t(t) - V_t(t-\Delta t)\right]/\Delta t$, respectively, and Δt is the sampling period.

Since $n(t)$ and its regressive values are unmeasurable, the input $\boldsymbol{\Phi}(t)$ cannot be obtained directly from voltage and current. In this context, the noise is estimated before identifying the parameters $\boldsymbol{\theta}(t)$ at each time index. The regressive values of the noise $n(t-i)$ can be estimated through the residual of the measured outputs and estimated outputs based on Eq. (5):

$$\hat{n}(t-i) = y(t-i) - \hat{\boldsymbol{\Phi}}^T(t-i)\hat{\boldsymbol{\theta}}(t-i) \tag{7}$$

where $i = 1, 2, \ldots, n_d$. In this way, the input $\boldsymbol{\Phi}(t)$ can be approximated by,

$$\hat{\boldsymbol{\Phi}}(t) = \left[I(t), \frac{dI(t)}{dt}, \frac{dV_t(t)}{dt}, \hat{n}(t-1), \ldots, \hat{n}(t-n_d)\right]^T \tag{8}$$

The initialization of the inputs and parameters can be set as

$$\hat{\boldsymbol{\Phi}}(1) = \hat{\boldsymbol{\Phi}}(2) = \cdots = \hat{\boldsymbol{\Phi}}(n_d) = \boldsymbol{\Phi}_0 \tag{9}$$

$$\hat{\boldsymbol{\theta}}(1) = \hat{\boldsymbol{\theta}}(2) = \cdots = \hat{\boldsymbol{\theta}}(n_d) = \boldsymbol{\theta}_0 \tag{10}$$

where the first three terms in $\boldsymbol{\Phi}_0$ are initialized through the measured data and the estimated noises in $\boldsymbol{\Phi}_0$ are initialized as

$$\hat{n}(1) = \hat{n}(2) = \cdots = \hat{n}(n_d) = 0 \tag{11}$$

According to ref. [30], $\boldsymbol{\theta}_0$ should be sufficiently small and therefore can be set as,

$$\boldsymbol{\theta}_0 = \left[10^{-6}, 10^{-6}, \cdots, 10^{-6}\right] \tag{12}$$

After obtaining the inputs, the parameters of the model can be identified timely through the following iterations:

$$\hat{\boldsymbol{\theta}}(t)=\hat{\boldsymbol{\theta}}(t-1)+\mathbf{P}(t)\hat{\boldsymbol{\Phi}}(t)\left[y(t)-\hat{\boldsymbol{\Phi}}^{T}(t)\hat{\boldsymbol{\theta}}(t-1)\right] \quad (13)$$

$$\mathbf{P}(t)=\frac{1}{\lambda}\left[\mathbf{P}(t-1)-\frac{\mathbf{P}(t-1)\hat{\boldsymbol{\Phi}}(t)\hat{\boldsymbol{\Phi}}^{T}(t)\mathbf{P}(t-1)}{\lambda+\hat{\boldsymbol{\Phi}}^{T}(t)\mathbf{P}(t-1)\hat{\boldsymbol{\Phi}}(t)}\right] \quad (14)$$

where $\mathbf{P}(t)$ is the gain factor and can be initialized as,

$$\mathbf{P}(1)=\mathbf{P}(2)=\cdots=\mathbf{P}(n_d)=p_0\mathbf{E} \quad (15)$$

in which p_0 is a large positive number (10^6 in this study), $\mathbf{E}$ is an identity matrix, $\lambda(0.95<\lambda<1)$ is a user-defined forgetting factor and is set to be 0.99 in this work.

With the identified parameters, the total internal resistance of the battery R_t at the time step t can be extracted as,

$$R_t=R_0+R_1=\theta_1(t) \quad (16)$$

R_t is used as the temperature-related feature to indicate battery SOT for the ML model introduced below.

C. The CNN-LSTM Model

Many mature ML algorithms such as ANNs, with high flexibility and performance, have received great attention in battery state estimations and health prognostics [10], [31]. CNNs and recurrent neural networks (RNNs), as two representatives of ANNs, exhibit great advantages in handling complex tasks. CNNs are capable of extracting the spatial information hidden in the original inputs through convolution and pooling, while RNNs are good at recognizing temporal patterns of data. LSTM, as an improved version of RNN, can solve the problems faced by conventional RNNs such as exploding and vanishing gradients by introducing the memory cell, as well as input and output gates [32]. Recently, there is a growing trend to combine these two networks to achieve higher performance by taking advantage of their respective strengths [33].

In this study, the ML algorithm is used to estimate the battery surface temperature based on multiple time-series signals and features. The estimation itself is a time-series task since the temperature at the current time step can be affected by the previous status and inputs [21]. Meanwhile, there also exist underlying relationships between the input signals such as current, voltage, and SOC. Therefore, to explore the relationship between input battery data and its temporal characteristics, CNN-LSTM is leveraged to yield the final estimation result based on these inputs. The structure of the proposed CNN-LSTM network is illustrated in Fig. 2. The time-series battery data with an input length of 15 is fed into the CNN-LSTM network. A CNN layer, consisting of a 1D convolution layer and a pooling layer, is used to extract the spatial features of the input data and then produce some high-level features. The number of filters (or kernels) used in the convolutional layer is 24 and the size of each kernel is chosen to be 3. Average pooling is adopted in the pooling layer and the kernel size is also 3. After capturing the spatial features of the input, an LSTM layer with a hidden size of 100 is applied to learn the temporal characteristics of these high-level features. The LSTM layer is followed by a fully connected (FC) layer with 50 neurons. Since this is a regression task, the final layer has only one neuron with the estimated surface temperature as the output. Generally, these hyperparameters of the CNN-LSTM model are tuned by trial and error. For instance, when determining the number of neurons in each layer, a small number can be tried at first and then increased gradually until a satisfactory performance is achieved [10].

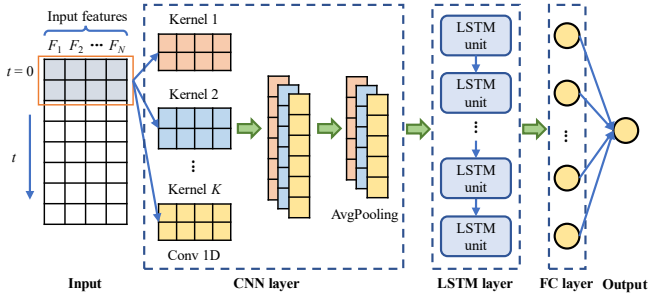

Fig. 2. Structure of the proposed CNN-LSTM for surface temperature estimation.

The CNN-LSTM was built and run based on the *Pytorch* library and the Adam optimizer was used during training to minimize the mean square error loss function, defined as,

$$MSE=\frac{1}{N}\sum_{i=1}^{N}(\hat{y}_i-y_i)^2 \quad (17)$$

where N is the number of samples in the training set, $\hat{y}_i$ and y_i are the output of the network and the truth value of the i-th sample, respectively.

D. Integration of Physics with ML

To combine the advantages of physics-based models and ML algorithms, the CNN-LSTM network is integrated sequentially with the lumped-mass thermal model to realize accurate and sensorless estimation of battery surface temperature, as

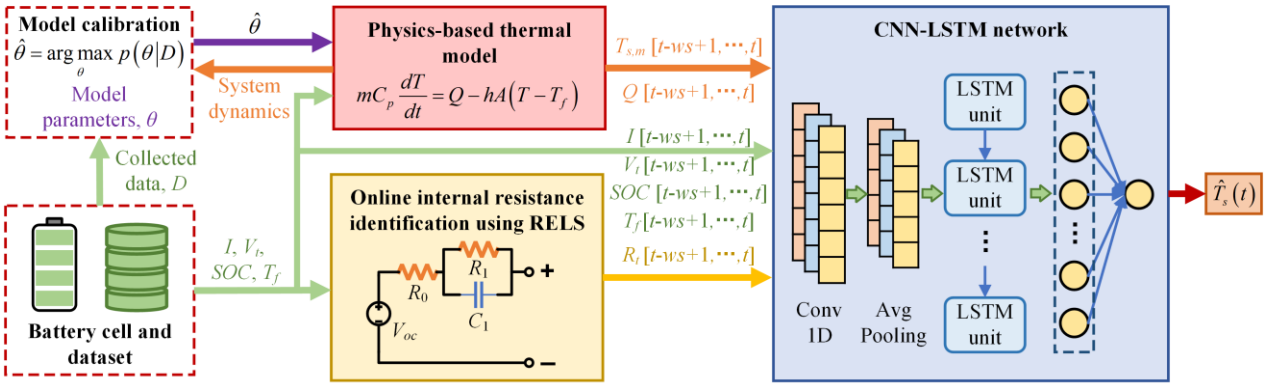

Fig. 3. Framework of integrating physics with CNN-LSTM for surface temperature estimation.

illustrated in Fig. 3. During the offline training process, battery data will be collected to parameterize the physics-based thermal model, as well as train the CNN-LSTM network. With system dynamics provided by the thermal model, the model parameters θ can be identified based on the collected data D as,

$$\hat{\theta} = \arg\max_{\theta} p\left(\theta | D\right) \tag{18}$$

where the parameters that need to be identified in the lumped-mass thermal model include heat capacity C_p and convection coefficient h. For control-oriented battery thermal modeling, these two thermal parameters are usually assumed to be constant [25]. Existing studies have also indicated slight changes in these two parameters under different operating conditions (i.e., temperature and SOC) and battery SOH [34], [35]. It should be noted that the calibration of the thermal model and the training of the CNN-LSTM network are based on the same collected data D.

During the online implementation stage, the measured current, voltage, SOC, and coolant temperature from the BMS, will flow into the thermal model block, resistance identification block, and CNN-LSTM network block. The parameterized thermal model calculates the heat generation Q and generates a prior estimation of the surface temperature $T_{s,m}$ according to the input. Both $T_{s,m}$ and Q are fed into the CNN-LSTM network as input. Since this lumped-mass thermal model might neglect some thermal dynamics inside the cell and have parameter uncertainties, the cumulative effect of these errors will cause the calculated surface temperature to deviate from the real value. However, despite errors, this calculated value can still be used as the prior temperature knowledge for the CNN-LSTM network, since it is able to track the general temperature trends. With this calculated temperature, the problem mentioned by Ojo et al. could be addressed, where the pure data-driven model was found unable to estimate battery surface temperature accurately when the prior knowledge of battery temperature was lacking [10]. Apart from the information provided by the physics-based model, some temperature-related features can be extracted from the original measurement and used as supplementary input to CNN-LSTM to further improve the estimation accuracy. Since the internal resistance R_t of the battery is temperature-dependent, it can be identified in real time based on the BMS measurements through the RELS algorithm to reflect the current battery SOT. As for the CNN-LSTM network, it not only receives the measured signals but also the prior information provided by the thermal model and the identified internal resistance. With such time-series information as input, the CNN-LSTM can generate a more accurate estimation of battery surface temperature $\hat{T}_s(t)$.

III. Description of Experimental Data

A publicly available experimental dataset has been used in this paper to validate the proposed surface temperature estimation method. The dataset was collected from the University of Wisconsin Madison [36] and the details of

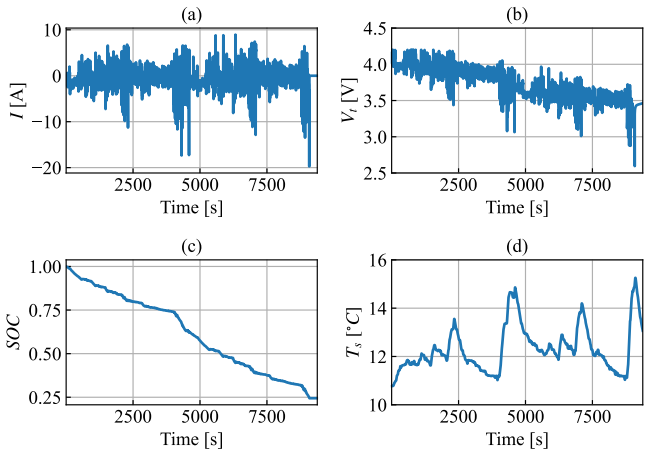

Fig. 4. The measured data during Cycle 1 under 10 °C. (a) Current, (b) Voltage, (c) SOC, (d) Surface temperature.

TABLE I
Summary of The Experimental Dataset [36]

Testing cycles	Ambient conditions
US06, HWFET, UDDS, LA92, Cycle 1, Cycle 2, Cycle 3, Cycle 4, NN	Fixed ambient temperatures: −20 °C, −10 °C, 0 °C, 10 °C, 25 °C Varying ambient temperatures: Starts from −20 °C and 10 °C
CC charge and discharge at 1/20 C	25 °C

experiments were described in ref. [37]. The test equipment includes a battery tester, a thermal chamber, and a host computer. A 2.9-Ah Panasonic 18650PF cell with lithium nickel cobalt aluminum oxide (NCA) chemistry was used for the test. The temperature at the middle surface of the cell was measured by a thermocouple and used as the surface temperature. The dataset covers a series of tests under a wide ambient temperature range (from −20 °C to 25 °C). At each test temperature, the cell was tested using different driving cycles from the fully charged state until the cell reached its cut-off voltage, namely 2.5 V. Standard driving cycles, such as Highway Fuel Economy Test (HWFET), Los Angeles 92 (LA92), Urban Dynamometer Driving Schedule (UDDS), and Supplemental Federal Test Procedure Driving Schedule (US06), were applied to the test. In addition, some synthesized cycles with the random mix of US06, HWFET, UDDS, and LA92 were also used to test the cell and these cycles include Cycle 1, Cycle 2, Cycle 3, Cycle 4, and Neural Network (NN). Apart from the tests at fixed ambient temperatures, experiments were also conducted at varying ambient temperatures which started from −20 °C or 10 °C and drifted upwards in steps. The OCV of the battery was tested at 25 °C by cycling the cell with a constant current (CC) of 1/20 C. All the tests of this battery cell, including different ambient temperatures and driving profiles, are summarized in Table I.

It should be noted that the original dataset was collected with a sampling frequency of 10 Hz. In this paper, however, the original data is preprocessed with a sampling frequency of 1 Hz, which is close to the real-world scenarios. Furthermore, to remove the noise in the temperature data, a Gaussian-weighted moving average filter with a window length of 40 is used and the filtered temperature is used as the true value. An illustration

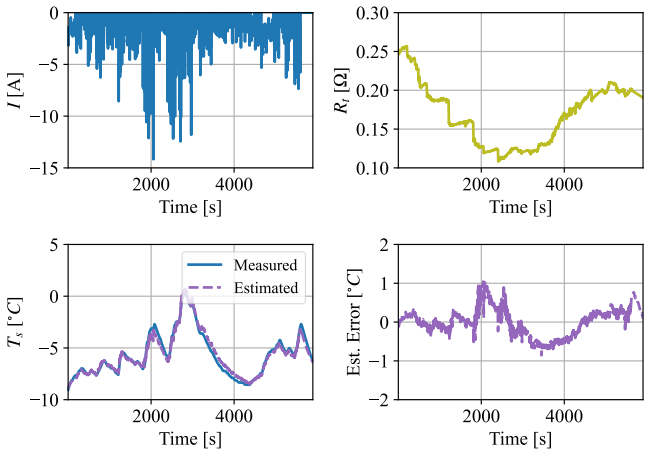

Fig. 5. Current, the identified resistance, the estimation result of the surface temperature, and the estimation errors of Cycle 2 under fixed ambient of −10 °C.

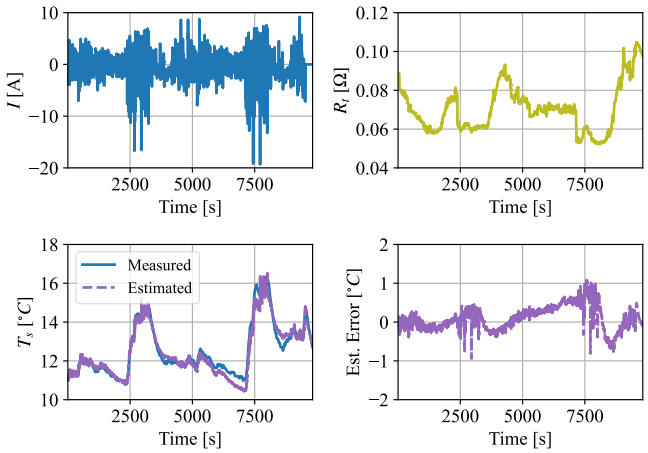

Fig. 6. Current, the identified resistance, the estimation result of the surface temperature, and the estimation errors of Cycle 4 under fixed ambient of 10 °C.

of the experimental data under Cycle 1 at the fixed ambient of 10 ℃ can be shown in Fig. 4.

IV. Results and Discussion

To train the proposed hybrid model, half of the driving cycles at different ambients, including two standard driving cycles (HWFET and LA92) and two synthesized cycles (Cycle 1 and Cycle 3), are used as the training data. The other driving cycles are used to test the accuracy of the estimation method. It should be noted that the tested battery in this experimental dataset is placed in the thermal chamber with air cooling, and therefore the ambient temperature is used as the coolant temperature when implementing the proposed method. In addition, since the RELS needs some time to converge, the data in the beginning 60 s of each driving cycle is not used as the input to the estimation framework to avoid the effect of unreasonable R_t on estimation results. All the inputs to the CNN-LSTM are normalized between [0,1] to eliminate the differences in the order of magnitude between input features. To train the CNN-LSTM, the training epoch is set as 2000, and the learning rate is 0.001. The training process stops when there is no significant decrease in the loss function to avoid overfitting.

The accuracy of the estimation can be evaluated through root mean square error (RMSE), mean absolute error (MAE), and maximum error (MAX), which are defined as follows:

$$RMSE = \sqrt{\frac{1}{K}\sum_{t=1}^{K}\left(T_s(t)-\hat{T}_s(t)\right)^2} \tag{19}$$

$$MAE = \frac{1}{K}\sum_{t=1}^{K}\left|T_s(t)-\hat{T}_s(t)\right| \tag{20}$$

$$MAX = Max\left|T_s(t)-\hat{T}_s(t)\right| \tag{21}$$

where K is the length of data in a testing cycle. Smaller values of these three metrics indicate better estimation accuracy.

TABLE II
Parameters of the Lumped-Mass Thermal Model

m	A	C_p	h
47 g	4.263×10^{-3} m^2	1.219 $J/(g\cdot K)$	25.3154 $W/(m^2\cdot K)$

TABLE III
Estimation Results with the Proposed Method at Fixed Ambient

Ambient conditions	Driving profiles	Error metrics		
		RMSE (℃)	MAE (℃)	MAX (℃)
−10 ℃	Cycle 2	0.37	0.29	1.04
	Cycle 4	0.37	0.29	1.18
	NN	0.42	0.29	1.57
	UDDS	0.24	0.20	0.76
	US06	1.14	1.02	2.11
10 ℃	Cycle 2	0.36	0.23	1.56
	Cycle 4	0.32	0.25	1.13
	NN	0.25	0.19	1.28
	UDDS	0.40	0.36	1.02
	US06	0.42	0.35	1.61

A. SOT Estimation at Fixed Ambient Temperatures

In this study, only one model is developed to estimate the surface temperature of batteries under different driving profiles and ambient conditions. The training dataset is used to not only train the CNN-LSTM network but also identify the parameters in the lumped-mass thermal model. The thermal model parameters, including the mass m, surface area A, heat capacity C_p, and convection coefficient h, are listed in Table II, with the first two parameters obtained from the battery data sheet and the latter two from identification. To examine the performance of the proposed SOT estimation method, the developed model is first tested at fixed ambient conditions using various driving cycles. Fig. 5 and Fig. 6 illustrate the estimation results at −10 ℃ and 10 ℃, respectively, where the current of the driving profile, the real-time internal resistance identified through the RELS algorithm, the estimated and measured temperatures, and the estimation errors are included. It is also worth noting that at low temperatures (i.e., below 10 ℃) the charging current due to regenerative braking is not included in the experiments, since the battery is not recommended to charge at that low-temperature range according to its specifications [37]. Although the modified testing current profiles at low temperatures are different from typical real-world cases with regenerative braking, accurate estimation of battery temperature under dynamic discharge currents still has great significance, which is of particular importance to the battery warm-up process in cold climates [5].

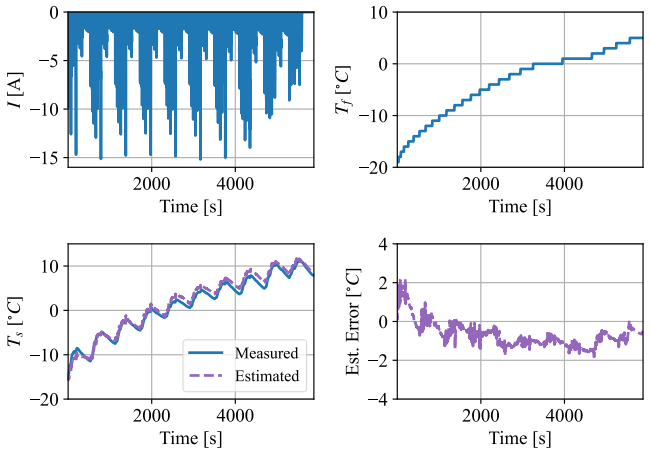

Fig. 7. Current, ambient temperature, the estimation result of the surface temperature, and the estimation errors of NN driving cycle under varying ambient starting −20 °C.

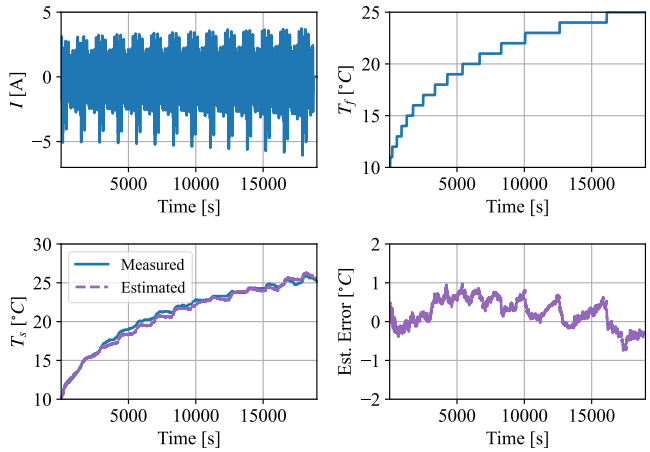

Fig. 8. Current, ambient temperature, the estimation result of the surface temperature, and the estimation errors of UDDS driving cycle under varying ambient starting 10 °C.

As can be seen from Fig. 5, the maximum temperature rise of the battery is almost 10 ℃ under Cycle 2 at −10 ℃ ambient due to the increased battery resistance at low temperatures. The internal resistance R_t, which is identified in real-time, may vary with battery SOC and temperature in one driving cycle. It can be seen from the identification result that generally R_t exhibits an opposite variation trend with battery temperature. That is, the internal resistance decreases with the rise of cell temperature and increases when the cell temperature declines, which demonstrates the effectiveness of the extracted temperature-related feature. Although R_t can also be influenced by battery SOC, such a hidden relationship can be captured by the CNN-LSTM since both SOC and R_t are used in the inputs. As such, the effect of this relationship on temperature estimation can be further eliminated. With the original measurements (i.e., current, voltage, coolant temperature, and SOC), the prior knowledge provided by the thermal model, and the extracted temperature-related feature as input, the CNN-LSTM network can achieve high estimation accuracy. The estimation error of surface temperature is basically within ±1 ℃ during the whole driving cycle, and the RMSE of the estimation is 0.37 ℃.

At 10 ℃, due to the decrease in internal resistance, the maximum temperature rise of the cell under Cycle 4 is around 5 ℃. The identified internal resistance in this case is much smaller than that at −10 ℃ but also shows an opposite variation trend with the cell temperature. It can be shown in Fig. 6 that the proposed method still achieves accurate estimation of battery SOT, with the estimation error within ±1 ℃ most of the time and RMSE of 0.32 ℃. To further verify the accuracy and generalization of the proposed method, the trained model is tested against more driving cycles under fixed ambients of −10 ℃ and 10 ℃, and the estimated results are summarized in Table III. For most driving cycles, both the RMSE and MAE of estimations are below 0.5 ℃, and the MAX can be kept within 2 ℃, demonstrating good accuracy and generalization ability of the proposed method. At −10 ℃, the SOT estimation error under US06 driving cycle is higher than that in other cycles, which could be caused by the significantly larger current and temperature rise compared to those cycles in the training set.

TABLE IV
ESTIMATION RESULTS WITH THE PROPOSED METHOD AT VARYING AMBIENT CONDITIONS

Ambient conditions	Driving profiles	Error metrics		
		RMSE (℃)	MAE (℃)	MAX (℃)
Intermittently increasing ambient temperature which starts from −20 ℃	Cycle 2	0.51	0.35	1.32
	Cycle 4	0.58	0.45	1.63
	NN	0.92	0.82	2.21
	UDDS	0.48	0.41	1.12
	US06	1.96	1.82	3.04
Intermittently increasing ambient temperature which starts from 10 ℃	Cycle 2	0.25	0.19	0.72
	Cycle 4	0.25	0.18	0.72
	UDDS	0.42	0.36	0.98

B. SOT Estimation at Varying Ambient Temperatures

In addition to the operations at fixed ambient temperatures, the battery system in electric mobilities can be subjected to coolant with varying temperatures in real-world scenarios due to the existence of the thermal management system. To verify the applicability of the proposed method under real-world situations, driving cycles with varying ambient temperatures are also used to test the model. Fig. 7 and Fig. 8 illustrate the estimation results at two different ambient conditions, where the ambient temperature starts to increase intermittently from −20 ℃ and 10 ℃, respectively. The current of the driving profile, the ambient temperature, the estimated and measured temperatures, and the estimation errors are presented in the results. In the ambient where the temperature increases gradually, the internal heat generation and the reduced heat dissipation contribute to a remarkable battery temperature rise compared to that in the fixed ambient case. The results in Fig. 7 and Fig. 8 show that the estimation errors are basically within ±2 ℃ and ±1 ℃, for the battery operations starting from −20 ℃ and 10 ℃ respectively. More driving cycles under varying ambient temperatures are applied to test the accuracy and generalization of the trained model, and the estimation performance can be summarized in Table IV, where in most cases the RMSE and MAE can be within 1 ℃, and MAX can be within 2 ℃.

This article has been accepted for publication in IEEE Transactions on Transportation Electrification. This is the author's version which has not been fully edited and content may change prior to final publication. Citation information: DOI 10.1109/TTE.2023.3294417

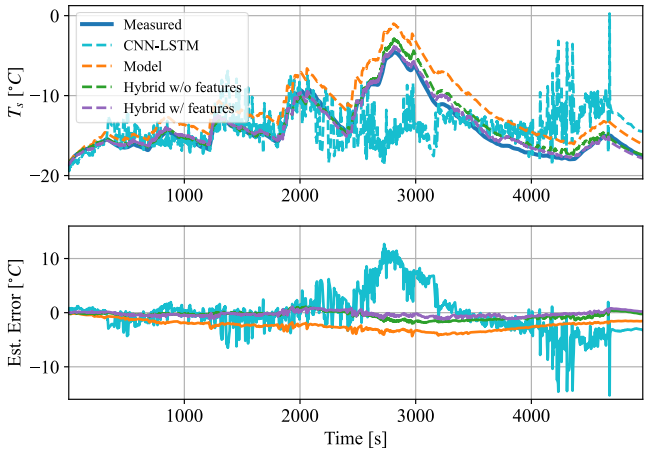

Fig. 9. Comparison of different estimation methods under Cycle 2 driving cycle at −20 °C.

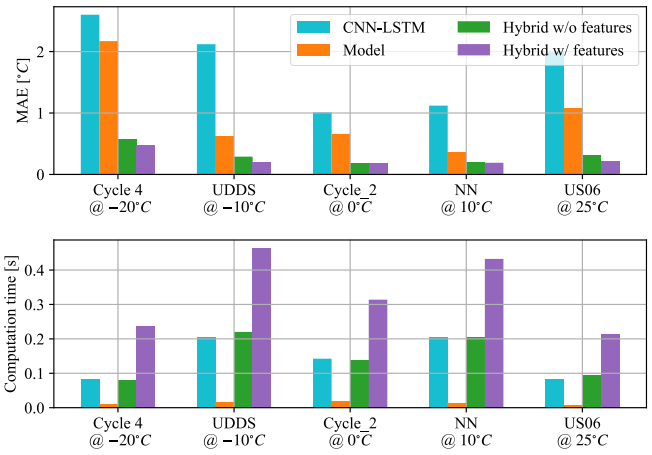

Fig. 10. Comparison of the four estimation methods under different driving cycles and ambient conditions in terms of their estimation accuracy and computation time.

TABLE V
COMPARISON OF ESTIMATION ACCURACY WITH DIFFERENT METHODS UNDER CYCLE 2 WITH A FIXED AMBIENT CONDITION OF −20 °C

Estimation methods	Input to CNN-LSTM	Error metrics		
		RMSE (°C)	MAE (°C)	MAX (°C)
Pure data-driven	[I, V_t, SOC, T_f]	3.78	2.67	15.29
Pure model-based	[I, V_t, SOC, T_f]	2.52	2.34	4.34
Hybrid w/o features	[I, V_t, SOC, T_f, $T_{s,m}$]	0.83	0.65	2.00
Hybrid w/ features	[I, V_t, SOC, T_f, $T_{s,m}$, Q, R_t]	0.52	0.45	1.22

C. Comparison of Different Methods

In this part, the proposed surface temperature estimation method is compared with conventional approaches. Four methods, namely the pure data-driven estimation, pure thermal model-based estimation, the hybrid method without temperature-related features in the input, and the hybrid method with temperature-related features in the input (i.e., the proposed method), are compared in terms of their performance in surface temperature estimation. Fig. 9 illustrates the comparison results under Cycle 2 at a fixed ambient condition of −20 °C as an example and the estimation errors of these four methods are summarized in Table V. As can be concluded from the results, the pure data-driven method using original measurements (i.e., [I, V_t, SOC, T_f]) as input has the worst accuracy among these four approaches. It is hypothesized that there is a poor correlation between the 15-s inputs and surface temperature. The same problem has also been identified by ref. [10], where the poor estimation performance of a two-layer LSTM-RNN (with the same input as the pure data-driven method in this paper) was ascribed to the lack of prior knowledge of battery temperature. As a consequence, although the loss function can be reduced to a low level during the training process, the trained CNN-LSTM network still has poor estimation performance in the testing dataset. As for the lumped-mass thermal model, owing to the uncertainties in thermal parameters and heat generation calculation, the temperature estimated by the thermal model will deviate from the real value. Specifically, the thermal parameters identified under one operating condition may not be able to capture battery thermal dynamics under other conditions, and therefore lead to increased estimation errors. As for the hybrid estimation, since it receives prior knowledge of battery temperature from the thermal model, the estimation error can be greatly reduced compared with the pure data-driven and the pure model-based methods, with accuracy improvement of 86.24% and 79.37% respectively. The CNN-LSTM network in the hybrid model can learn from the error between the thermal model output and the real surface temperature, and then reduce this error. The supplementation of temperature-related features such as internal resistance and heat generation can further improve the estimation accuracy by 37.35% in contrast to the hybrid method without these features.

In order to compare the four methodologies comprehensively, various driving cycles at different ambient conditions are used to examine these methods in terms of their computational complexity and generalization capability. To this end, the computation time and the MAE of these four methods are recorded in different testing cycles. The result of the comparison can be illustrated in Fig. 10. As can be seen from the results, the proposed hybrid method achieves significantly higher estimation accuracy compared to pure data-driven estimation and pure thermal model-based estimation in all the testing scenarios, indicating good generalization capability. Adding temperature-related features can further improve the estimation accuracy in most driving cycles. In terms of computation complexity, the pure thermal model-based estimation has the least computation time due to its simple model structure. The hybrid method without temperature-related features as input has comparable computational complexity with pure data-driven method, since the computational cost added by the thermal model is negligible. As for the hybrid method with temperature-related features in the input, computation time is the highest, which is caused by the online identification of battery internal resistance. Therefore, whether temperature-related features should be involved in the estimation or not depends on the computational capability of the BMS as well as the accuracy requirement. Generally, the involvement of the neural network will bring extra computational burdens to the BMS. To alleviate such

computational burden faced by the microprocessor, the neural network in the proposed method can be further optimized to be more lightweight and efficient, without sacrificing too much estimation accuracy. For example, Bayesian optimization, as an excellent paradigm, can be applied to determine the optimal hyperparameters of the neural network such as the input length, as well as the number of layers and hidden neurons in the future instead of empirical hyperparameter tuning [38].

V. Conclusion

This paper proposes a sensorless surface temperature estimation method for LIBs by combing a physics-based thermal model with ML algorithms. In this estimation framework, a lumped-mass thermal model is integrated sequentially with the CNN-LSTM network. The temperature calculated by the thermal model serves as the prior knowledge of battery temperature. With this prior information, the CNN-LSTM network can achieve an accurate estimation of surface temperature. Moreover, the internal resistance of the cell, which could be used as a direct indicator of battery SOT, is identified from the current and voltage in a real-time manner and treated as supplementary input to the network to improve the estimation accuracy. The proposed method has been validated under various large current profiles and extreme ambient conditions, with RMSE less than 1 ℃ and MAX less than 2 ℃ in most cases, even under subzero ambient where the battery cell has a significant temperature rise. A comparison of different methodologies indicates that the proposed method outperforms pure data-driven and pure model-based estimations. By adding the identified internal resistance and heat generation rate in the CNN-LSTM inputs, the estimation accuracy can be further improved. The proposed method can be applied to real-time estimation and monitoring of the battery temperature without temperature sensors.

VI. Future work

The methodology in this article is developed based on fresh battery data without considering battery aging, which makes it challenging to achieve effective temperature monitoring in the long term. Particularly, since the internal resistance of the battery is not only dependent on operating conditions (i.e., temperature and SOC) but also SOH, the rise of the internal resistance due to battery aging will increase the estimation error when applying the same algorithm to estimate battery temperature. However, compared to the resistance change caused by operating conditions, the internal resistance change as a result of battery aging is a slow process and such change can be negligible in dozens of cycles [39], [40]. In real-world applications, the CNN-LSTM network can be updated periodically over time by taking advantage of the temperature data measured by the sparsely arranged temperature sensors in the battery pack, to make the algorithm adaptive to battery aging. Therefore, future work will be conducted to update the neural network at different aging statuses to achieve effective and long-term temperature monitoring.

References

[1] J. B. Goodenough and K.-S. Park, "The Li-Ion Rechargeable Battery: A Perspective," *J Am Chem Soc*, vol. 135, no. 4, pp. 1167–1176, Jan. 2013, doi: 10.1021/ja3091438.

[2] J. T. Frith, M. J. Lacey, and U. Ulissi, "A non-academic perspective on the future of lithium-based batteries," *Nature Communications*, vol. 14, no. 1. Nature Research, Dec. 01, 2023. doi: 10.1038/s41467-023-35933-2.

[3] V. Viswanathan *et al.*, "The challenges and opportunities of battery-powered flight," *Nature*, vol. 601, no. 7894. Nature Research, pp. 519–525, Jan. 27, 2022. doi: 10.1038/s41586-021-04139-1.

[4] X. Feng, M. Ouyang, X. Liu, L. Lu, Y. Xia, and X. He, "Thermal runaway mechanism of lithium ion battery for electric vehicles: A review," *Energy Storage Materials*, vol. 10. Elsevier, pp. 246–267, Jan. 01, 2018. doi: 10.1016/j.ensm.2017.05.013.

[5] X. Hu, Y. Zheng, D. A. Howey, H. Perez, A. Foley, and M. Pecht, "Battery warm-up methodologies at subzero temperatures for automotive applications: Recent advances and perspectives," *Prog Energy Combust Sci*, vol. 77, 2020, doi: 10.1016/j.pecs.2019.100806.

[6] J. S. Edge *et al.*, "Lithium ion battery degradation: what you need to know," *Physical Chemistry Chemical Physics*, vol. 23, no. 14. pp. 8200–8221, 2021. doi: 10.1039/d1cp00359c.

[7] J. Lin, X. Liu, S. Li, C. Zhang, and S. Yang, "A review on recent progress, challenges and perspective of battery thermal management system," *Int J Heat Mass Transf*, vol. 167, p. 120834, Mar. 2021, doi: 10.1016/j.ijheatmasstransfer.2020.120834.

[8] X. Lin, H. E. Perez, J. B. Siegel, and A. G. Stefanopoulou, "Robust estimation of battery system temperature distribution under sparse sensing and uncertainty," *IEEE Transactions on Control Systems Technology*, vol. 28, no. 3. pp. 753–765, 2020. doi: 10.1109/TCST.2019.2892019.

[9] R. R. Richardson, P. T. Ireland, and D. A. Howey, "Battery internal temperature estimation by combined impedance and surface temperature measurement," *J Power Sources*, vol. 265, pp. 254–261, 2014, doi: 10.1016/j.jpowsour.2014.04.129.

[10] O. Ojo, H. Lang, Y. Kim, X. Hu, B. Mu, and X. Lin, "A Neural Network Based Method for Thermal Fault Detection in Lithium-Ion Batteries," *IEEE Transactions on Industrial Electronics*, vol. 68, no. 5, pp. 4068–4078, 2021, doi: 10.1109/TIE.2020.2984980.

[11] N. Wang *et al.*, "Core Temperature Estimation Method for Lithium-ion Battery Based on Long Short-term Memory Model with Transfer Learning," *IEEE J Emerg Sel Top Power Electron*, vol. PP, no. 2019, p. 1, 2021, doi: 10.1109/JESTPE.2021.3136906.

[12] X. Tang, K. Yao, B. Liu, W. Hu, and F. Gao, "Long-Term Battery Voltage, Power, and Surface Temperature Prediction Using a Model-Based Extreme Learning Machine," *Energies (Basel)*, vol. 11, no. 1, p. 86, Jan. 2018, doi: 10.3390/en11010086.

[13] X. Du, J. Meng, J. Peng, Y. Zhang, T. Liu, and R. Teodorescu, "Sensorless Temperature Estimation of Lithium-ion Battery based on Broadband Impedance Measurements," *IEEE Trans Power Electron*, vol. PP, no. c, pp. 1–1, 2022, doi: 10.1109/tpel.2022.3166170.

[14] X. Wang *et al.*, "A review of modeling, acquisition, and application of lithium-ion battery impedance for onboard battery management," *eTransportation*, vol. 7, p. 100093, Feb. 2021, doi: 10.1016/j.etran.2020.100093.

[15] S. Ludwig, I. Zilberman, M. F. Horsche, T. Wohlers, and A. Jossen, "Pulse resistance based online temperature estimation for lithium-ion cells," *J Power Sources*, vol. 490, p. 229523, 2021, doi: 10.1016/j.jpowsour.2021.229523.

[16] P. Rodríguez-Iturriaga, D. Anseán, J. A. López-Villanueva, M. González, and S. Rodríguez-Bolívar, "A method for the lifetime sensorless estimation of surface and core temperature in lithium-ion batteries via online updating of electrical parameters," *J Energy Storage*, vol. 58, Feb. 2023, doi: 10.1016/j.est.2022.106260.

[17] R. R. Richardson and D. A. Howey, "Sensorless Battery Internal Temperature Estimation Using a Kalman Filter with Impedance Measurement," *IEEE Transactions on Sustainable Energy*, vol. 6, no. 4. pp. 1190–1199, 2015. doi: 10.1109/TSTE.2015.2420375.

[18] Y. Xie *et al.*, "An Enhanced Online Temperature Estimation for Lithium-Ion Batteries," *IEEE Transactions on Transportation Electrification*, vol. 6, no. 2, pp. 375–390, 2020, doi: 10.1109/TTE.2020.2980153.

[19] G. Cho, M. Wang, Y. Kim, J. Kwon, and W. Su, "A Physics-Informed Machine Learning Approach for Estimating

Lithium-Ion Battery Temperature," *IEEE Access*, vol. 10. Institute of Electrical and Electronics Engineers Inc., pp. 88117–88126, 2022. doi: 10.1109/ACCESS.2022.3199652.

[20] M. Naguib, P. Kollmeyer, and A. Emadi, "Application of Deep Neural Networks for Lithium-Ion Battery Surface Temperature Estimation Under Driving and Fast Charge Conditions," *IEEE Transactions on Transportation Electrification*, 2022, doi: 10.1109/TTE.2022.3200225.

[21] Q. Yao, D. D. C. Lu, and G. Lei, "A Surface Temperature Estimation Method for Lithium-ion Battery Using Enhanced GRU-RNN," *IEEE Transactions on Transportation Electrification*, 2022, doi: 10.1109/TTE.2022.3197927.

[22] L. H. J. Raijmakers, D. L. Danilov, J. P. M. Van Lammeren, M. J. G. Lammers, and P. H. L. Notten, "Sensorless battery temperature measurements based on electrochemical impedance spectroscopy," *J Power Sources*, vol. 247, pp. 539–544, 2014, doi: 10.1016/j.jpowsour.2013.09.005.

[23] J. P. Schmidt, S. Arnold, A. Loges, D. Werner, T. Wetzel, and E. Ivers-Tiffée, "Measurement of the internal cell temperature via impedance: Evaluation and application of a new method," *J Power Sources*, vol. 243, pp. 110–117, 2013, doi: 10.1016/j.jpowsour.2013.06.013.

[24] H. Pang, L. Guo, L. Wu, J. Jin, F. Zhang, and K. Liu, "A novel extended Kalman filter-based battery internal and surface temperature estimation based on an improved electro-thermal model," *J Energy Storage*, vol. 41, no. June, p. 102854, 2021, doi: 10.1016/j.est.2021.102854.

[25] X. Hu, W. Liu, X. Lin, and Y. Xie, "A Comparative Study of Control-Oriented Thermal Models for Cylindrical Li-Ion Batteries," *IEEE Transactions on Transportation Electrification*, vol. 5, no. 4. pp. 1237–1253, 2019. doi: 10.1109/TTE.2019.2953606.

[26] Y. Xu, S. Kohtz, J. Boakye, P. Gardoni, and P. Wang, "Physics-informed machine learning for reliability and systems safety applications: State of the art and challenges," *Reliab Eng Syst Saf*, vol. 230, Feb. 2023, doi: 10.1016/j.ress.2022.108900.

[27] H. Liu, Z. Wei, W. He, and J. Zhao, "Thermal issues about Li-ion batteries and recent progress in battery thermal management systems: A review," *Energy Convers Manag*, vol. 150, no. August, pp. 304–330, 2017, doi: 10.1016/j.enconman.2017.08.016.

[28] D. Bernardi, E. Pawlikowski, and J. Newman, "A General Energy Balance for Battery Systems," *J Electrochem Soc*, vol. 132, no. 1, pp. 5–12, Jan. 1985, doi: 10.1149/1.2113792.

[29] T. Feng, L. Yang, X. Zhao, H. Zhang, and J. Qiang, "Online identification of lithium-ion battery parameters based on an improved equivalent-circuit model and its implementation on battery state-of-power prediction," *J Power Sources*, vol. 281, pp. 192–203, May 2015, doi: 10.1016/j.jpowsour.2015.01.154.

[30] F. Ding and T. Chen, "Identification of Hammerstein nonlinear ARMAX systems," *Automatica*, vol. 41, no. 9, pp. 1479–1489, Sep. 2005, doi: 10.1016/j.automatica.2005.03.026.

[31] Y. Che, Z. Deng, X. Lin, L. Hu, and X. Hu, "Predictive Battery Health Management with Transfer Learning and Online Model Correction," *IEEE Trans Veh Technol*, vol. 70, no. 2, pp. 1269–1277, Feb. 2021, doi: 10.1109/TVT.2021.3055811.

[32] S. Hochreiter, "The Vanishing Gradient Problem During Learning Recurrent Neural Nets and Problem Solutions," *International Journal of Uncertainty, Fuzziness and Knowledge-Based Systems*, vol. 06, no. 02, pp. 107–116, Apr. 1998, doi: 10.1142/S0218488598000094.

[33] L. Ren, J. Dong, X. Wang, Z. Meng, L. Zhao, and M. J. Deen, "A Data-Driven Auto-CNN-LSTM Prediction Model for Lithium-Ion Battery Remaining Useful Life," *IEEE Trans Industr Inform*, vol. 17, no. 5, pp. 3478–3487, May 2021, doi: 10.1109/TII.2020.3008223.

[34] M. Steinhardt, J. v. Barreras, H. Ruan, B. Wu, G. J. Offer, and A. Jossen, "Meta-analysis of experimental results for heat capacity and thermal conductivity in lithium-ion batteries: A critical review," *Journal of Power Sources*, vol. 522. Elsevier B.V., Feb. 28, 2022. doi: 10.1016/j.jpowsour.2021.230829.

[35] J. Geder, R. Arunachala, S. Jairam, and A. Jossen, "Thermal behavior of aged lithium-ion batteries: calorimetric observations," in *2015 IEEE Green Energy and Systems Conference (IGESC)*, IEEE, Nov. 2015, pp. 24–29. doi: 10.1109/IGESC.2015.7359386.

[36] P. Kollmeyer, "Panasonic 18650pf li-ion battery data," *Mendeley Data*, vol. 1, no. 2018, 2018.

[37] E. Chemali, P. J. Kollmeyer, M. Preindl, R. Ahmed, and A. Emadi, "Long Short-Term Memory Networks for Accurate State-of-Charge Estimation of Li-ion Batteries," *IEEE Transactions on Industrial Electronics*, vol. 65, no. 8, pp. 6730–6739, Aug. 2018, doi: 10.1109/TIE.2017.2787586.

[38] B. Shahriari, K. Swersky, Z. Wang, R. P. Adams, and N. De Freitas, "Taking the human out of the loop: A review of Bayesian optimization," *Proceedings of the IEEE*, vol. 104, no. 1. Institute of Electrical and Electronics Engineers Inc., pp. 148–175, Jan. 01, 2016. doi: 10.1109/JPROC.2015.2494218.

[39] J. Guo *et al.*, "Unravelling and quantifying the aging processes of commercial $Li(Ni_{0.5}Co_{0.2}Mn_{0.3})O_2$ /graphite lithium-ion batteries under constant current cycling," *J Mater Chem A Mater*, vol. 11, no. 1, pp. 41–52, 2023, doi: 10.1039/D2TA05960F.

[40] S. Barcellona, S. Colnago, G. Dotelli, S. Latorrata, and L. Piegari, "Aging effect on the variation of Li-ion battery resistance as function of temperature and state of charge," *J Energy Storage*, vol. 50, p. 104658, Jun. 2022, doi: 10.1016/j.est.2022.104658.